Mechanism of Activation of Human Heparanase Investigated by Protein Engineering†

Caterina Nardella, Armin Lahm, Michele Pallaoro, Mirko Brunetti, Alessandro Vannini, and Christian Steinkühler*

Department of Biochemistry, IRBM/Merck Research Laboratories, Via Pontina Km, 30600 Pomezia, Italy

Received September 11, 2003; Revised Manuscript Received November 24, 2003

ABSTRACT: The aim of this study was to investigate the mechanism of activation of human heparanase, a key player in heparan sulfate degradation, thought to be involved in normal and pathologic cell migration processes. Active heparanase arises as a product of a series of proteolytic processing events. Upon removal of the signal peptide, the resulting, poorly active 65 kDa species undergoes the excision of an intervening 6 kDa fragment generating an 8 kDa polypeptide and a 50 kDa polypeptide, forming the fully active heterodimer. By engineering of tobacco etch virus protease cleavage sites at the N- and C-terminal junctions of the 6 kDa fragment, we were able to reproduce the proteolytic activation of heparanase in vitro using purified components, showing that cleavage at both sites leads to activation in the absence of additional factors. On the basis of multiple-sequence alignment of the N-terminal fragment, we conclude that the first $\beta/\alpha/\beta$ element of the postulated TIM barrel fold is contributed by the 8 kDa subunit and that the excised 6 kDa fragment connects the second β-strand and the second α-helix of the barrel. Substituting the 6 kDa fragment with the topologically equivalent loop from *Hirudinaria manillensis* hyaluronidase or connecting the 8 and 50 kDa fragments with a spacer of three glycine-serine pairs resulted in constitutively active, single-chain heparanases which were comparable to the processed, heterodimeric enzyme with regard to specific activity, chromatographic profile of hydrolysis products, complete inhibition at NaCl concentrations above 600 mM, a pH optimum of pH ∼5, and inhibition by heparin with IC_{50}s of 0.9−1.5 ng/μL. We conclude that (1) the heparanase heterodimer $(\alpha/\beta)_8$-TIM barrel fold is contributed by both 8 and 50 kDa subunits with the 6 kDa connecting fragment leading to inhibition of heparanase by possibly obstructing access to the active site, (2) proteolytic excision of the 6 kDa fragment is necessary and sufficient for heparanase activation, and (3) our findings open the way to the production of recombinant, constitutively active single-chain heparanase for structural studies and for the identification of inhibitors.

Heparanase is a recently cloned protein (*1*−*4*) involved in binding to and degradation of heparan sulfate (HS)[1] which is the polysaccharide component of heparan sulfate proteoglycans (HSPGs) present on the cell surface and extracellular matrix (ECM) (*5*−*10*). In the extracellular milieu, HSPGs play crucial structural (*5*−*8*) and regulatory roles (*11*−*18*), modulating important normal and pathological processes ranging from embryogenesis, morphogenesis, and development (*19*) to inflammation, angiogenesis, and cancer metastasis (*20*, *21*). HS cleavage by heparanase allows cells to migrate through the basal membranes (BM) and traverse the ECM barriers. Heparanase has in fact been identified in normal and malignant invading cells ranging from activated cells of the immune system and placental trophoblasts to metastatic tumor cells, such as lymphoma, melanoma, and carcinoma cells (*22*−*26*). Several lines of evidence suggest the involvement of heparanase in the process of tumor metastasis. Metastatic tumor cells but not all tumors upregulate heparanase activity, and an increased level of heparanase mRNA expression correlates with invasiveness of tumor cells (*1*, *2*, *22*, *25*, *27*). This correlation was confirmed by showing that transfection and overexpression of the heparanase gene in nonmetastatic cell types result in the acquisition of a metastatic behavior (*1*). On the other side, transfection with heparanase antisense cDNA in cells expressing the ectopic heparanase gene results in the inhibition of the increased metastatic potential (*28*). Apart from its role in cell extravasation from blood vessels and migration through the ECM, heparanase activity has been demonstrated to promote tumor growth and angiogenesis releasing growth factors, such as fibroblast growth factors (FGF1 and FGF2), vascular endothelial growth factor (VEGF), hepatocyte growth factor, transforming growth factor β, and platelet-derived growth factor (*13*), that are normally stored by HS in the ECM (*26*, *29*−*31*). It has been also suggested that, independent of its enzymatic activity and depending on the local pH, heparanase may be involved in cell adhesion (*32*, *33*) emphasizing, therefore, the importance of this protein in the cell−extracellular environment interface.

† This work was partially supported by a grant from MIUR.

* To whom correspondence should be addressed: Department of Biochemistry, IRBM/Merck Research Laboratories, Via Pontina Km 30,600, 00040 Pomezia, Italy. Phone: +39 06 91093232. Fax: +39 06 91093225. E-mail: christian_steinkuhler@merck.com.

[1] Abbreviations: *bla*, β-lactamase gene; DMEM, Dulbecco's modified Eagle's medium; ECM, extracellular matrix; FBS, fetal bovine serum; FITC, fluorescein isothiocyanate; FITC-HS, FITC-labeled heparan sulfate; HAB, heparanase activity buffer; Hepes, *N*-(2-hydroxyethyl)piperazine-*N*′-2-ethanesulfonic acid; HPLC, high-pressure liquid chromatography; HS, heparan sulfate; HSPGs, heparan sulfate proteoglycans; Mes, 2-(*N*-morpholino)ethanesulfonic acid; PBS, phosphate-buffered saline; SDS−PAGE, sodium dodecyl sulfate−polyacrylamide gel electrophoresis; TEV, tobacco etch virus; Tris, tris(hydroxymethyl)aminomethane.

10.1021/bi030203a CCC: $27.50
Published on Web 01/30/2004

Because of this pivotal role, heparanase is a potential novel target for the development of antitumor, antimetastasis, or anti-inflammatory drugs. Exploiting heparanase as a drug target is presently hampered by both the scarcity of reliable high-throughput assays and its complex biogenesis, which renders the production of large amounts of active protein a difficult task.

Human heparanase cDNA encodes a protein that is initially synthesized as a pre-pro-protein with a signal peptide sequence (residues Met1−Ala35) removed by signal peptidase upon translocation into the endoplasmic reticulum. The resulting 65 kDa pro form is further processed by removing the 157 N-terminal amino acids to yield the mature 50 kDa heparanase (*1*, *2*). The 50 kDa protein has a specific activity at least 100-fold higher than that of the unprocessed 65 kDa precursor (*1*). Interestingly, the 50 kDa protein is inactive if expressed as such in mammalian cells (*2*), and the active form of the enzyme was proposed to be a heterodimer between the 50 kDa fragment and an 8 kDa fragment arising from the excision of an intervening 6 kDa peptide (residues Glu109−Gln157) by unidentified proteolytic enzyme(s) (*34*). Recently, evidence in this respect was furnished by the work of McKenzie et al. (*35*) and by Levy-Adam et al. (*36*), who were able to produce active heterodimeric heparanase and confirmed that the 8 kDa subunit is necessary for heparanase activity. Still, the role of the 8 kDa subunit in the activation process of heparanase is unclear: it might function as an essential subunit or, alternatively, act as a chaperone and then be dispensable. Also, it is not clear whether other components besides the 8 kDa subunit are necessary to elicit heparanase activation. Multiple-sequence alignments and secondary structure prediction lead to a model of the human heparanase according to which the protein adopts a TIM barrel fold, as found in several glycosidases (*37*). This common fold motif usually consists of eight alternating α-helices and β-strands. Within the 50 kDa fragment, clear homology is observed only starting with the third α/β unit of the TIM barrel fold, suggesting either that heparanase adopts a novel fold consisting of only six α/β units or that other parts of the protein contribute the missing units. A possible candidate here is the 8 kDa fragment, which might contribute the missing structural elements. Following this hypothesis, we built a model of the secondary structure of heparanase, based on multiple-sequence alignments, to design single-chain heparanase molecules having the 8 and 50 kDa subunits covalently linked together. We show that grafting of a loop derived from *Hirudinaria manillensis* hyaluronidase or connecting the two fragments with three glycine-serine repeats resulted in constitutively active, single-chain heparanase molecules. By engineering tobacco etch virus protease cleavage sites at the N- and C-termini of the 6 kDa fragment, we further show that proteolytic processing at both sites of a purified protein leads to activation in the absence of other components. Our findings provide evidence of human heparanase adopting a canonical TIM barrel fold and open the way to facile production of active enzyme molecules for the identification of specific inhibitors.

MATERIALS AND METHODS

Cloning of Heparanase from a Human Placenta cDNA Library. Human heparanase (AF155510) was amplified from a normal human placenta cDNA library (Invitrogen SRL, Milan, Italy) by PCR using TaKaRa La Taq polymerase (Takara Shuzo Co., Ltd.). Buffer conditions were those suggested by the supplier, and reaction mixtures were cycled as follows: 94 °C for 1 min and 35 cycles of 94 °C for 30 s, 57 °C for 30 s, and 68 °C for 110 s. The amplified fragment was gel purified, phosphorylated, and cloned either in the *Bam*HI site of pFAST BAC1, after filling in (baculovirus expression), or into a *Bam*HI−*Eco*RI-digested pCDNA3 vector (mammalian cell expression). The following primers were used for amplification and simultaneous optimization of the Kozak sequence: hHEP1−24 BamHI opti, cgg gat ccg ccg cac cat gct gct gcg ctc gaa gcc tgc g; hHEP rev 1632, tca gat gca agc agc aac ttt ggc.

Sequence Analysis and Structure Prediction. Proteins whose sequences are significantly similar with that of human heparanase were identified using BLAST (*38*) searches against publicly available peptide and nucleic acid sequence databases. Secondary structure prediction was performed using the PSIPRED prediction algorithm (*39*). Sequences were initially aligned using CLUSTALW (*40*), and the alignment was subsequently manually optimized using the SEAVIEW program (*41*), taking into account the predicted secondary structure and the structural features of the TIM barrel fold. Sequences reported in the alignment are as follows: HEPAR_HUMAN (Refseq entry NP_006656, *Homo sapiens*), HEPAR_MOUSE (Refseq entry NP_690016, *Mus musculus*), HEPAR_BOSTAU (Refseq entry NP_776507, *Bos taurus*), HEPAR_GALLUS (Genpept entry AAK82648, *Gallus gallus*), HEPLIKE_HUMAN (Refseq entry NP_068600, *H. sapiens*), HEPLIKE_BM (Genpept entry BAB85191, *Bombyx mori*), HYALURON_HM (Genpept entry CAC22595, *Hirudinaria manillensis*), BETA-GLUCOR_SB (Genpept entry BAA97804, *Scutellaria baicalensis*), ARAB_NP_196400 (Refseq entry NP_196400, *Arabidopsis thaliana*), ARAB_NP_851093 (Refseq entry NP_851093, *A. thaliana*), and ARAB_NP_900233 (Refseq entry NP_900233, *A. thaliana*).

Construction of Single-Chain Heparanase Molecules. The following constructs (WT, hep109, hep106, hepGS3, hepGS/A4, hepGS/A6, and hepHyal), covalently linking the 8 and 50 kDa subunits in a direct fashion (hep109 and hep106), linking the subunits via glycine-serine spacers (hepGS3) or via glycine-serine/alanine spacers (hepGS/A4 and hepGS/A6), or linking the subunits by grafting a loop region from the *H. manillensis* hyaluronidase (hepHyal), were generated by standard PCR mutagenesis using the indicated primers: hHEP1−24 BamHI opti, cgg gat ccg ccg cac cat gct gct gcg ctc gaa gcc tgc g (forward primer); hHEP rev 1632, tca gat gca agc agc aac ttt ggc (reverse primer); hep109, M1...E109−Q157...I543, hHEP 304/504 forw, cta att ttc gat ccc aag aag gaa aaa aag ttc aag aac agc acc tac (mutagenic primer); hep106, M1...P106−K158...I543, hHEP 291/504 bis forw, aag aca gac ttc cta att ttc gat ccc aaa aag ttc aag aac agc acc tac (mutagenic primer); hepGS3, M1...E109-$(GS)_3$-Q157...I543, hHEP 304(GS3)504 forw, cta att ttc gat ccc aag aag gaa ggt agc ggt tcc ggc tct aaa aag ttc aag aac (mutagenic primer); hepGS/A4, M1...W118-$(GS/A)_4$-E143...I543, hHEP 329(GS4 ALA) forw, acc ttt gaa gag aga agt tac tgg ggt tca ggg gca gga tcc ggc gcc gaa tgg ccc tac cag gag caa ttg (mutagenic primer); hepGS/A6**,** M1...E109-$(GS/A)_6$-Q157...I543, hHEP 304(GS6 ALA) forw, cta att ttc gat ccc aag aag gaa ggt agc ggc gct gga tca ggg gca gga tcc ggc gcc aaa aag ttc aag aac

agc acc tac (mutagenic primer); hepHyal, M1...W118-(AFKDKTP)-E143...I543, hHEP Hyaluro forw, acc ttt gaa gag aga agt tac tgg gcc ttc aag gac aag acc ccc gaa tgg ccc tac cag gag caa ttg (mutagenic primer).

Transient Expression in COS7 Cells. COS7 cells (monkey kidney fibroblast) were grown in Dulbecco's modified Eagle's medium (DMEM) (Gibco BRL, Life technologies Italia Srl, Milan, Italy). All constructs were cloned into the eukaryotic expression plasmid pcDNA3 (Invitrogen SRL). A vector encoding the reporter gene β-lactamase (*bla*) was cotransfected to check the transfection efficiency of each construct. The quantity of each transfected vector was adjusted to obtain comparable transfection efficiencies. Transient transfection of COS7 cells was obtained using the fuGENE 6 Transfection Reagent (Roche Diagnostics Spa, Milan, Italy) according to the manufacturer's instructions. Twenty-four hours after transfection, the efficiency was assessed by fluorimetric detection of *bla*-positive cells. Ninety-six hours after transfection, cells were harvested and resuspended in lysis buffer [50 mM Tris-HCl (pH 7.5), 150 mM NaCl, and 0.5% (v/v) Triton containing Complete protease inhibitor cocktail (Roche Diagnostics Spa)]. The lysis was carried out on ice for 30 min. After centrifugation at 14 000 rpm for 30 min, the heparanase-containing supernatants were recovered and purified as outlined below.

Expression in Insect Cells. Recombinant baculoviruses containing the heparanase constructs were generated using the Bac to Bac expression system. Recombinant baculoviruses were used to infect Sf9 insect cells (50×10^6 cells per T-175 flask) grown in Grace's insect medium (Gibco BRL, Life technologies Italia Srl) supplemented with 10% (v/v) FBS. Cells were collected 48 h after infection and centrifuged at 500*g* for 5 min. Cell lysates were prepared as described above using a lysis buffer with 500 mM NaCl instead of 150 mM NaCl, which was used for COS7 cells (here we used 500 mM NaCl because we observed an improvement in protein quantity in the soluble fraction). Finally, supernatants were diluted to 150 mM NaCl and were partially purified as outlined below.

Purification of Recombinant Heparanase Constructs on Heparin Sepharose. Cell lysates from COS7 or Sf9 cells were passed through a 500 μL heparin−Sepharose CL-6B column (Amersham Biosciences, Milan, Italy) by gravity. The column was washed with 2 mL of lysis buffer, and then with 2 mL of 50 mM Tris-HCl (pH 7.5) and 500 mM NaCl, and heparanase was eluted with 2 mL of 50 mM Tris-HCl (pH 7.5) and 1 M NaCl and concentrated ~5-fold with a Biomax-30K centrifugal concentrator (Millipore, Milan, Italy). Glycerol (10%, v/v) was added, and the protein was stored in aliquots at −80 °C. The protein concentration was determined using the Bio-Rad protein assay (Bio-Rad, Milan, Italy).

Western Blot Analysis. Rabbit polyclonal antibodies were generated by AnaSpec Inc. (San Jose, CA) against a peptide contained within the 50 kDa subunit (EPNSFLKKADIF-INGSQ, corresponding to amino acids 225−241 and containing an additional GGC sequence at its C-terminus). Antisera were immunopurified using the immunogenic peptide immobilized on a thiopropyl-Sepharose resin (Amersham Biosciences). Ten microliters of heparanase proteins eluted from the heparin column was subjected to 10% SDS−PAGE and transferred onto a Protran BA 83 cellulose nitrate membrane (Schleicher & Schuell Italia Srl, Milan, Italy). After saturation of nonspecific binding with 5% (w/v) milk, the membrane was incubated with the polyclonal antibody described above diluted 1:500 in 50 mM Tris (pH 7.5), 150 mM NaCl, 5% (w/v) milk, and 0.05% (v/v) Tween 20 overnight at 4 °C. After being washed, the membrane was incubated with anti-rabbit horseradish peroxidase-conjugated antibody diluted 1:5000 for 30 min at room temperature. The immunoreactive bands were detected by SuperSignal West Pico Chemiluminescent Substrate (Pierce). Finally, the membrane was exposed to Kodak BIOMAX MR film (Sigma-Aldrich Srl, Milan, Italy).

Fluorimetric Labeling of Heparan Sulfate. Heparan sulfate sodium salt from bovine kidney (Sigma-Aldrich Srl) was labeled with fluorescein isothiocyanate (FITC) (Sigma-Aldrich Srl) as previously described (*4*). Five milligrams of heparan sulfate and 5 mg of FITC were dissolved in 1 mL of 0.1 M Na_2CO_3 (pH 9.5), and the mixture was incubated overnight at 4 °C in the dark. The solution was then loaded on MicroSpin G-25 columns to separate FITC-labeled heparan sulfate (FITC-HS) from unreacted FITC. The FITC-HS was subjected to a first gel-filtration chromatographic step through Sephacryl S-300 in 150 mM NaCl and 25 mM Tris-HCl buffer (pH 7.5) to separate the high-molecular mass heparan sulfate species. The colored fractions were pooled, concentrated with a Biomax-10K centrifugal concentrator (Millipore), and rechromatographed on a Sephacryl S-300 column (as above) to obtain heparan sulfate species with homogeneous molecular masses. The eluted fractions were analyzed with an HPLC Superdex 75 (Amersham Biosciences) chromatography system. The fluorescence in each fraction was measured with an L-7485 fluorimetric detector (Merck-Hitachi). We obtained four main fractions with different molecular mass heparan sulfate products. The quantity of FITC-HS in each fraction was measured with the Blyscan glycosaminoglycan assay (Biocolor Ltd., Belfast, Northern Ireland).

Fluorimetric Assay. This assay, as previously described (*4*), is based on the degradation of FITC-HS monitored by HPLC size exclusion chromatography. Heparanase was incubated with approximately 1 μg of FITC-HS in 50 μL of 50 mM Mes (pH 6) and 10% (v/v) glycerol [heparanase activity buffer (HAB)]. The reaction mixture was incubated at room temperature for a defined period of time, and the reaction was stopped by the addition of 50 μg of heparin. The mixture was then filtered using Ultrafree-MC centrifugal filter devices (Millipore); 20 μL was injected on a Superdex 75 (Amersham Biosciences) column equilibrated in 50 mM Hepes (pH 7.5) and 150 mM Na_2SO_4 and connected to a Merck-Hitachi HPLC system. Fluorescent heparan sulfate degradation products were detected with an L-7485 fluorescence detector with excitation at 492 nm and emission at 524 nm. Heparanase activity was assessed by monitoring the increase in the amount of the lower-molecular mass heparan sulfate species compared with the amount of intact FITC-HS and quantified by peak area integration. We observed that this assay is linear with respect to time (insets in Figure 5a−c) or the amount of enzyme (data not shown).

Radiometric Labeling and Biotinylation at the Reducing End of Heparan Sulfate. Ten milligrams of heparan sulfate sodium salt from bovine kidney (Sigma-Aldrich Srl) was partially deacetylated and reacetylated with [^{3}H]acetic an-

hydride as previously described (*42*). Tritiated heparan sulfate was then subjected to reductive amination at the reducing end as described previously (*43*). Tritiated, reductively aminated heparan sulfate was further conjugated to biotin using EZ-Link Sulfo-NHS-LC-Biotin (Pierce, Perbio Science Europe). This biotin analogue has an *N*-hydroxysuccinimido ester moiety that can react with the amino group generated at the reducing end of the heparan sulfate molecules. We calculated a recovery of ~5 mg of tritiated heparan sulfate, reductively aminated and resuspended in 1 mL of H_2O. To 100 μL of this solution were added 1 mg of EZ-Link Sulfo-NHS-LC-Biotin and 20 μL of 50 mM phosphate buffer (pH 7.5). The reaction mixture was incubated overnight at room temperature. The reaction mixture was then loaded on a PD-10 desalting column to isolate biotinylated, tritiated heparan sulfate from unreacted biotin. We finally obtained four fractions (1 mL each), which were tested for their ability to be immobilized on Reacti-Bind Streptavidin High Binding Capacity Coated Plates (Pierce, Perbio Science Europe).

Radiometric Assay. This assay is based on the degradation of tritiated heparan sulfate immobilized on a microplate. Each well of the Reacti-Bind Streptavidin High Binding Capacity Coated Plates was pretreated according to the manufacturer's instructions. Initially, different amounts of each fraction of tritiated, biotinylated heparan sulfate obtained after using the PD-10 desalting column were added to each well (in duplicate) in PBS and 0.05% (v/v) Tween 20 to a final volume of 100 μL. After we determined that the maximum binding is obtained with a volume of fraction 2 corresponding to 100×10^3 dpm, this amount was always used. The binding was carried out overnight at room temperature. The wells were then washed three times with PBS and 0.05% (v/v) Tween 20 and twice with HAB. Heparanase was added to each well in 100 μL of HAB. The wells were incubated at room temperature for 2−24 h. Finally, the liberated radioactivity due to tritiated heparan sulfate products generated by heparanase in each well was measured and normalized against a buffer blank.

Determination of the Specific Activity of Heparanase Constructs. Specific activities of the heparanase constructs either transiently expressed in COS7 cells or expressed in the baculovirus system were determined as follows:

$$\text{specific activity} = [\text{normalized activity (dpm}/\mu\text{L)}]/[\text{normalized densitometric volume (volume}/\mu\text{L)}]$$

In detail, activity of the partially purified heparanase constructs was determined in the radiometric assay by titrating each preparation in such a way that a linear dose−activity relationship was observed. These titrations were repeated three times with each preparation, and a mean, normalized activity (dpm/μL) was calculated. Protein expression was assessed by the Western blotting experiments: the chemiluminescent readout was quantified by densitometry using a model GS-700 imaging densitometer (Bio-Rad). Again, experiments were repeated three times, and mean values were determined. The specific activity was obtained by dividing the normalized activity (dpm/μL) by the normalized densitometric volume (volume/μL).

pH Dependence. To determine the optimum pH of heparanase activity toward FITC-HS, we carried out the enzymatic reaction as described for the fluorimetric assay method at various pH values ranging from 4.2 to 7. For each pH value, we used a three-component buffer containing 24.6 mM Mes, 24.6 mM acetate, 50 mM Tris, and the pH-dependent variations in ionic strength were corrected by addition of NaCl such that the final strength of all solutions was 50 mM. All solutions were further supplemented with 10% (v/v) glycerol. The reactions were carried out at room temperature for a time established for each heparanase construct in such a way that a linear time−activity relationship was observed. Heparanase activity was calculated by integrating chromatographic data as described above.

Ionic Strength Dependence. The ionic strength dependence of heparanase activity toward FITC-HS was assessed by carrying out the enzymatic reaction as described in the fluorimetric assay method at different concentrations of NaCl ranging from 160 mM to 1 M. Each reaction was conducted in HAB complemented with the appropriate concentration of NaCl. The reactions were conducted at room temperature for a time established for each heparanase construct in such a way that a linear time−activity relationship was observed. Heparanase activity was calculated by integrating chromatographic data as described above.

Inhibition by Heparin. The effect of heparin on heparanase activity toward FITC-HS was determined in the fluorimetric assay. Each reaction was carried out in HAB complemented with different concentrations of heparin sodium salt from porcine intestinal mucosa (Sigma-Aldrich Srl). The reactions were conducted at room temperature for a time established for each heparanase construct in such a way that a linear time−activity relationship was observed. Heparanase activity was calculated by integrating chromatographic data as described above and reported as the percentage of the maximum heparanase activity obtained in the absence of heparin.

Construction of Heparanase Molecules with Engineered Protease Cleavage Sites. To construct an engineered heparanase molecule in which the consensus cleavage site for the tobacco etch virus (TEV) protease flanked by GS repeats (E109-**GSGSENLYFQ-GSG**-G110, the scissile bond being located between Q and G) was inserted between amino acids E109 and G110 (this construct was named hepTEV110), PCR mutagenesis was employed using wild-type heparanase as a template and the following primers: hHEP1−24 *Bam*HI opti, cgg gat ccg ccg cac cat gct gct gcg ctc gaa gcc tgc g (forward primer); hHEP rev 1632, tca gat gca agc agc aac ttt ggc (reverse primer); TEV110 bis forw, ggc agc gga tct gag aac ctg tac ttc cag ggt tcc ggt tca acc ttt gaa gag aga agt tac (mutagenic primer).

To construct an engineered heparanase having TEV cleavage sites between residues E109 and G110 and between residues Q157 and K158 (this construct was named hepTEV110/158), the hepTEV110 construct was used as a template to insert the sequence Q157-**GSGSENLYFQ-GSGS**-K158 by PCR mutagenesis using the following mutagenic primer: TEV158 ter forw, tct gga tcc ggt gaa aat ctc tat ttt cag ggc tca gga agt aaa aag ttc aag aac agc acc tac.

All constructs were sequenced on both strands to ensure that no mutations were introduced by PCR and cloned into pFASTBAC1, and the recombinant baculoviruses were produced as described above.

Purification of hepTEV110 and hepTEV110−158 Constructs. These constructs were purified from the medium of

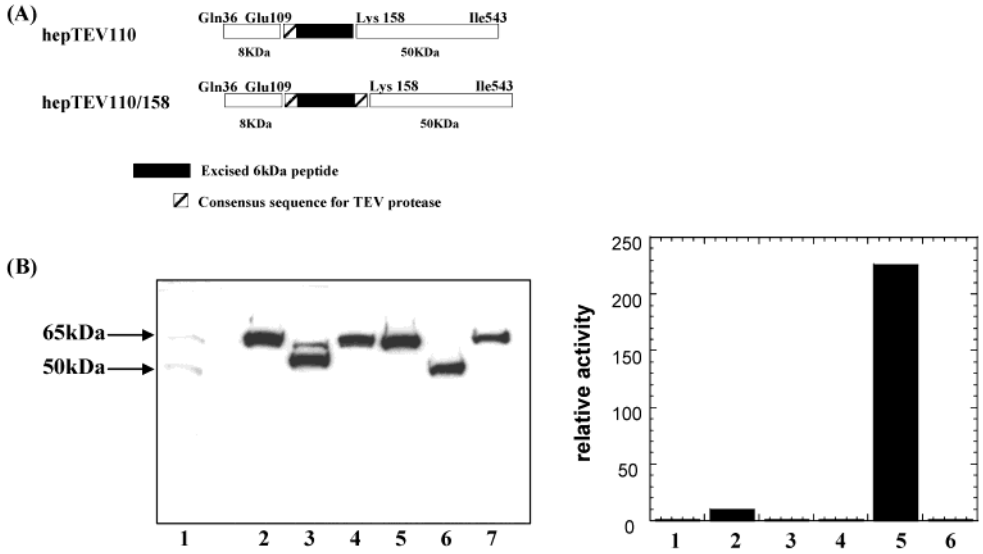

FIGURE 1: (A) Schematic view of the heparanase constructs with engineered TEV cleavage sites. (B) Western blot analysis of correctly processed wild-type heparanase expressed in COS7 cells (lane 1), hepTEV110 (lane 2), hepTEV110 after incubation for 16 h with (lane 3) or without (lane 4) 0.5 μM TEV protease, hepTEV110/158 (lane 5), and hepTEV110/158 after incubation for 16 h with (lane 6) or without (lane 7) 0.5 μM TEV protease (left). Heparanase activity of hepTEV110 (column 1), hepTEV110 after incubation for 16 h with (column 2) or without (column 3) 0.5 μM TEV protease, hepTEV110/158 (column 4), and hepTEV110/158 after incubation for 16 h with (column 5) or without (column 6) 0.5 μM TEV protease (right). The heparanase activity of these samples was assessed using the fluorimetric method.

the infected insect cells because we observed a larger amount of protein in the secreted form. Three hundred milliliters of medium [Grace's insect medium with 10% (v/v) FBS] of insect cells infected with recombinant baculovirus was passed through a 0.22 μm filter and loaded on a 20 mL HyperD heparin column (BioSepra, Ciphergen Biosystems Inc., Fremont, CA) equilibrated with 50 mM Tris-HCl (pH 7.5) and 150 mM NaCl using an FPLC system. Both heparanase constructs were eluted by applying a linear 0.15 to 1 M NaCl gradient in 50 mM Tris-HCl (pH 7.5). The two proteins eluted at an NaCl concentration of approximately 600 mM. The fractions were assayed by Western blot analysis; the ones containing a heparanase construct were pooled (32 mL) and concentrated using a Centriprep 30 000 molecular weight cutoff (Millipore) to a final volume of 2 mL. This 2 mL was dialyzed against 50 mM phosphate buffer (pH 7) and passed through a Mono S column (Amersham Biosciences) equilibrated in the same buffer using the FPLC system. These proteins were eluted with a linear 0 to 0.5 M NaCl linear gradient in 50 mM phosphate buffer (pH 7). The two constructs eluted with approximately 300 mM NaCl. The fractions were analyzed by 10% SDS−PAGE gels (Bio-Rad) followed by staining with Coomassie blue. Fractions containing heparanase constructs were pooled and supplemented with 10% (v/v) glycerol.

Digestion of hepTEV110 and hepTEV110/158 by TEV Protease. The hepTEV110 and hepTEV110/158 proteins were digested overnight at room temperature with TEV protease (0.5 μM) in 50 mM MES (pH 6), 10% (v/v) glycerol, and 0.5 mM EDTA in the presence of FITC-HS. The reaction mixture was divided into two aliquots: one supplemented with SDS loading buffer to stop TEV protease activity and then loaded on 10% SDS−PAGE gels (Bio-Rad) followed by Western blot analysis as described above and the other supplemented with heparin to stop heparanase activity toward FITC-HS and injected on a Superdex 75 (Amersham Biosciences) column connected to the HPLC system (see Fluorimetric Assay). The chromatographic data were integrated as described in Fluorimetric Assay.

RESULTS

Characterization of Heparanase Constructs Harboring the Tobacco Etch Virus Protease Consensus Sequence (hepTev110 and hepTev110/158). To address the question of whether proteolytic processing at the junctions between residues 109 and 110 and 157 and 158 is both necessary and sufficient to elicit activation of heparanase, we attempted to reproduce this reaction in vitro using purified components. Since the proteolytic enzymes involved in this process are unknown, we reasoned that the two cleavage sites (Glu109 and Gln157) by definition must be exposed, thus allowing alternative cleavage sites, accessible to known proteases, to be introduced. These variants could be expressed and purified, most likely in an inactive form, and subsequently activated, providing an exogenous protease. For this purpose, we generated constructs harboring cleavage sites for the tobacco etch virus (TEV) protease in the proximity of natural processing sites 110 and 158 (Figure 1A). The construct having the TEV protease cleavage site between positions 109 and 110 (hepTEV110) and the one having this site between positions 109 and 110 and 157 and 158 (hepTEV110/158) of the pro-heparanase 65 kDa form were cloned into the pFastBac vector. The recombinant baculoviruses were generated and used to infect Sf9 insect cells. These two constructs were purified from medium of infected insect cells by two sequential chromatographic steps over HyperD heparin and Mono S columns. Each construct, >90% pure, was digested with TEV protease in the presence of fluorescein-labeled heparan sulfate (FITC-HS), and the efficiency of the proteolytic cleavage was assessed by Western blot analysis (Figure 1B, left). In parallel, we analyzed the effect of the proteolytic cleavage on activation of heparanase enzymatic

activity toward FITC-HS (Figure 1B, right). From Western blot analysis, we concluded that both constructs were efficiently processed by TEV protease. The two constructs, when uncleaved, did not exhibit measurable heparanase activity. Also, cleavage by TEV protease of the construct harboring the TEV consensus sequence between positions 109 and 110 did not lead to a significant emergence of heparanase activity (Figure 1). In contrast, incubation with TEV protease of the construct harboring TEV consensus cleavage sites at both positions 109 and 110 and 157 and 158 led to pronounced activation of heparanase enzymatic activity. We conclude that processing after residue 109 is insufficient to elicit activation. In vitro processing at both sites, however, did lead to active heparanase, indicating that no other factors in addition to the processing reaction are required.

Design of Constitutively Active Heparanase. After reproducing the proteolytic activation of heparanase with purified components in vitro, we went on to further analyze the structural basis for the inactivity of the 65 kDa precursor. Following a combination of sequence analysis and structure prediction, the TIM barrel architecture, frequently observed in glycosylases, has been proposed to be present also in heparanase (*37*). Predicted secondary structure and sequence motifs conserved with respect to other glycosylases strongly support this hypothesis. Site-directed mutagenesis of the two principal catalytic residues, predicted on the basis of the TIM barrel hypothesis, was performed on both heparanase and a homologous β-glucuronidase from *Scutellaria baicalensis*, confirming the TIM barrel hypothesis (*37*).

The structure prediction did, however, not include the N-terminal portion of heparanase where the internal segment comprising residues Glu109−Gln157 is excised to activate the enzyme. Although variations in the number of (α/β) units actually present in TIM barrel structures have been observed, the vast majority of known or predicted TIM barrel structures conserve the classical $(\alpha/\beta)_8$ motif. A number of arguments favor heparanase being in this category. First, secondary structure predictions indicate the presence of a $\beta/\alpha/\beta$ element in the N-terminal 8 kDa fragment (Figure 2A). Like in a number of TIM barrel glycosylases with known structure, a completely conserved arginine residue is present inside the barrel on the second β-strand, presumably interacting with the catalytic Glu343 on β-strand 6. In this configuration, the excised segment would be located within the second β/α structural unit; more precisely, it should be inserted between the β-strand and the α-helix, which is predicted to be immediately downstream of the second cleavage site at Gln157.

Starting from this hypothesis and using a multiple alignment of sequences that are significantly similar with that of heparanase (Figure 2A), we set out to design a number of heparanase variants where the internal fragment is replaced by a much shorter loop (Figure 2B). If this approach was successful, single-chain heparanase variants without the need for activation would be generated. Apart from two designs where the internal segment is simply omitted, with or without the flanking cleavage sites (hep109 and hep106 in Figure 3A), we also generated three constructs using short Gly-Ser (hepGS3 in Figure 3A) or Gly-Ser-Gly-Ala linkers (hepGS/A4 and hepGS/A6 in Figure 3A) as replacements. Finally, we also decided to profit from the fact that other enzymes whose sequences are significantly similar to that of heparanase are known. Particularly interesting was *H. manillensis* hyaluronidase, detected in the patent nucleotide sequence database. The overall sequence of this enzyme was rather highly identical (~35%) to that of heparanase, and even more interestingly, this enzyme was reported to be active without processing (*44*). Since this hyaluronidase had a much shorter loop in the region under question, we decided to generate a chimera where most of the excised loop region in heparanase was replaced with the equivalent region in the *H. manillensis* enzyme. The precise crossover point was determined according to the sequence alignment (Figure 2A) substituting only the central portion of the loop with the much shorter hyaluronidase region (hepHyal in Figure 3A). An equivalent construct bearing instead a $(GlySer/Ala)_4$ linker was also designed. The various homologous plant enzymes, another alternative, were disfavored since they contain two conserved cysteines in the loop region under question, and it is not known if these form disulfide bonds with each other or with other cysteines of the protein.

Characterization of Heparanase Single-Chain Constructs in Mammalian Cells. We initially characterized the functionality of the heparanase single-chain proteins in mammalian cells. We cloned the wild-type full-length human heparanase cDNA (as a control) and the constructs encoding the heparanase single-chain proteins into the eukaryotic expression vector pcDNA3. These vectors were used to transiently transfect the COS7 mammalian cell line, which is devoid of detectable endogenous heparanase activity. Heparanase was extracted from cell lysates by heparin affinity chromatography and quantified by Western blotting (Figure 3B, left). In parallel, heparanase enzymatic activity was determined with either the radiometric (Figure 3B, right) or fluorimetric assay (data not shown).

On the Western blot, wild-type heparanase extracted from COS7 cells appeared as two bands: a minor one of ~65 kDa corresponding to the heparanase precursor and a major one of ~50 kDa corresponding to the processed form (Figure 3). The single-chain construct hepHyal, with the *H. manillensis* loop grafted onto heparanase, was efficiently expressed and processed as was the hepGS3 construct, whereas constructs hep106 and hepGS/A4 were expressed but not processed. Expression levels of constructs hep109 and hepGS/A6 were extremely low and could barely be detected by Western blot analysis (Figure 3).

Importantly, the hepHyal construct showed enzymatic activity comparable to that of the wild-type enzyme. Under these conditions, activity was also observed for the hepGS3 single-chain construct. In contrast, no other engineered heparanase exhibited any significant heparan sulfate degrading activity. Since the hepHyal construct (as well as the hepGS3 construct) is active but is also processed despite the changes that were introduced, we cannot draw any conclusion with respect to the intrinsic activity of the precursor, nor can we accurately determine specific activities under these conditions. We therefore proceeded with the expression of the wild-type full-length human heparanase and the single-chain constructs hepHyal and hepGS3 in insect cells that are devoid of the enzyme(s) responsible for heparanase processing.

Characterization of Heparanase Single-Chain Constructs in Insect Cells. Wild-type full-length human heparanase and

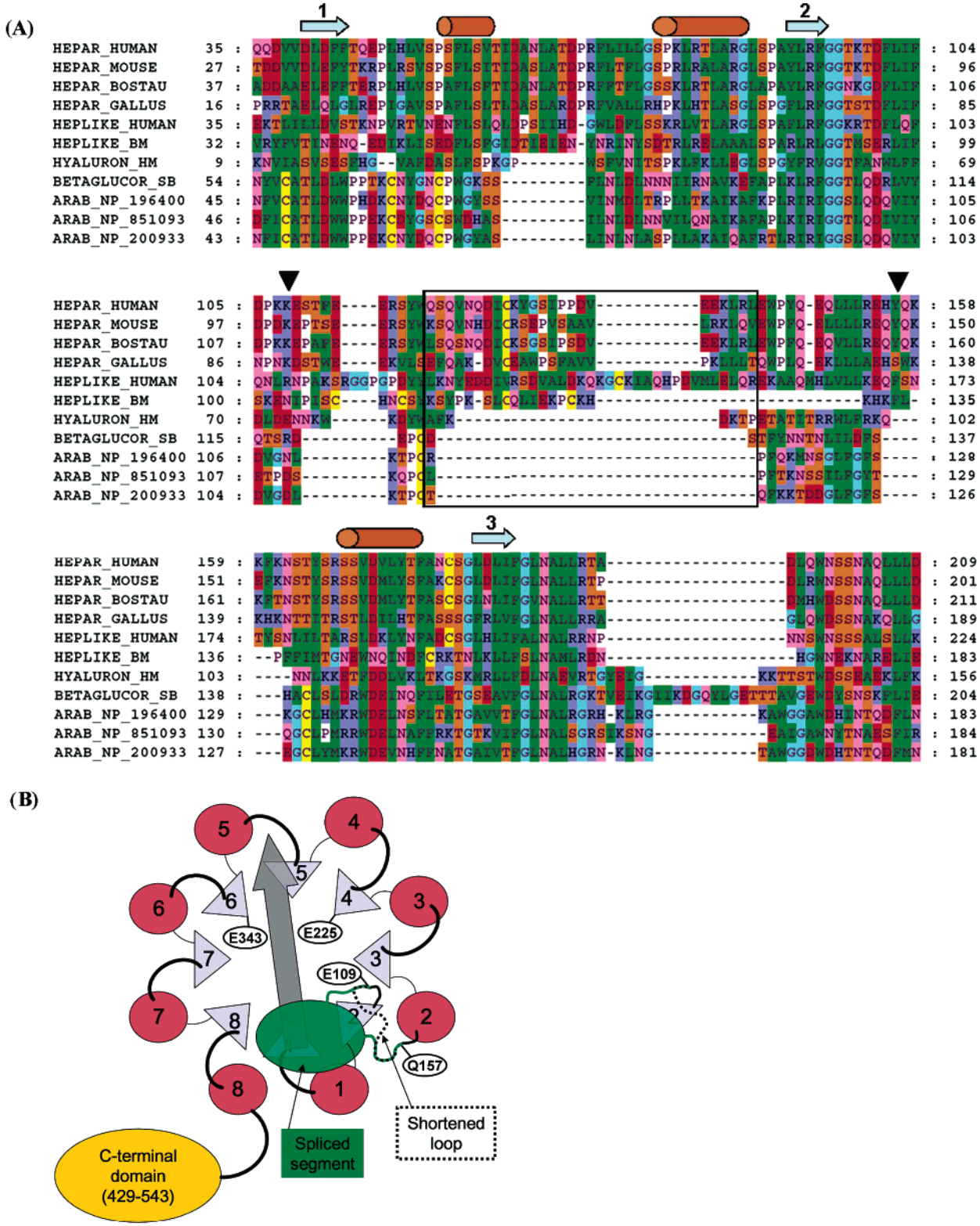

FIGURE 2: (A) Multiple-sequence alignment of heparanase against related sequences. Predicted secondary structure elements are shown above the alignment (arrows for β-strands and cylinders for α-helices). The positions of the two cleavage sites are denoted with black triangles. The region of the excised heparanase segment substituted with the *H. manillensis* hyaluronidase fragment is surrounded by a box. (B) Schematic view of the TIM barrel architecture. Loops connecting the β and α units are shown as thick (barrel face toward the viewer) or thin (opposite face of the barrel) lines. Conserved active site residues Glu225 and Glu343 are denoted. The location of the excised heparanase segment is indicated by green color, including cleavage points Glu109 and Gln157. When present, the segment most likely obscures binding of the substrate (gray arrow) by β/α units 1 and 2. Design of a shorter loop (dotted line) removes this constraint, leading to an active enzyme while, at the same time, maintaining the structural integrity of the barrel.

the single-chain constructs hepHyal and hepGS3, which exhibited enzymatic activity when expressed in COS7 cells, were transferred into the pFastBac vector; recombinant baculoviruses were obtained and were used to infect Sf9 insect cells. The cell lysates were purified on heparin affinity chromatography and then either analyzed by Western blotting

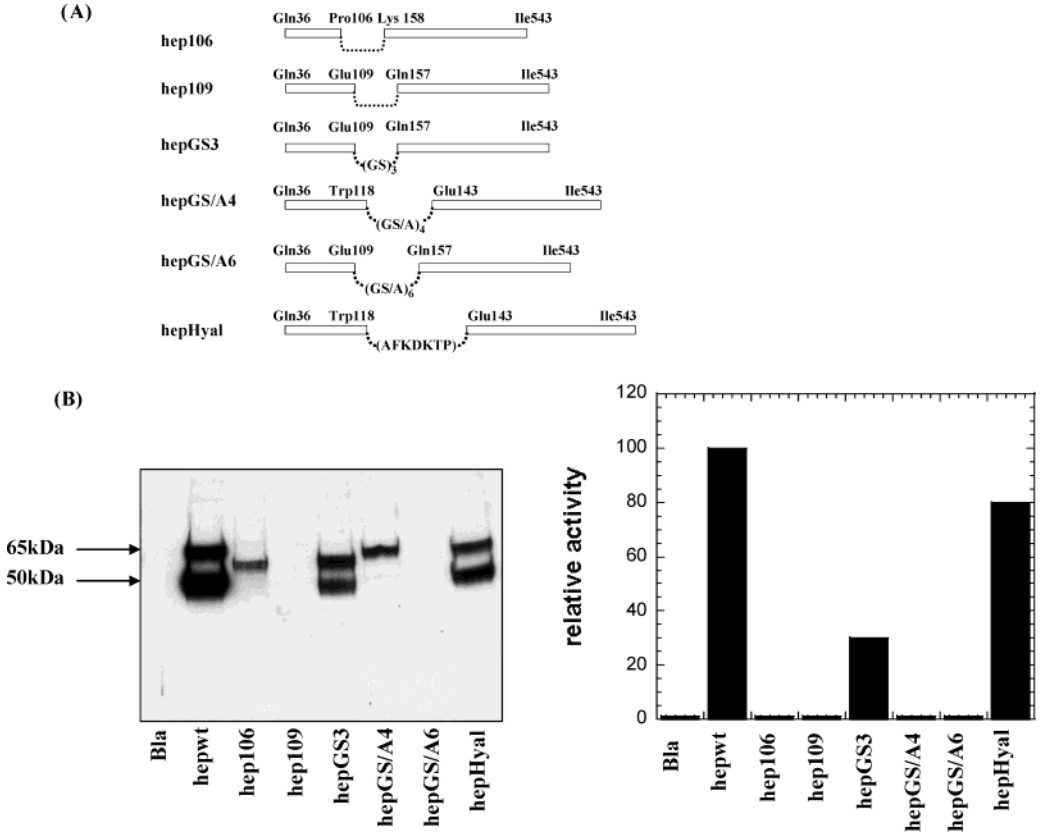

FIGURE 3: (A) Schematic view of the single-chain heparanase constructs. (B) At the left, Western blot analysis of wild-type heparanase or single-chain constructs expressed in COS7 cells. Bla is a control corresponding to the partially purified lysate of COS7 cells transfected only with a vector encoding the reporter gene β-lactamase (see Materials and Methods). At the right, heparanase activity of the same samples using the radiometric assay. The specific activity of all single-chain constructs is normalized against that of the wild-type heparanase and reported as relative activity.

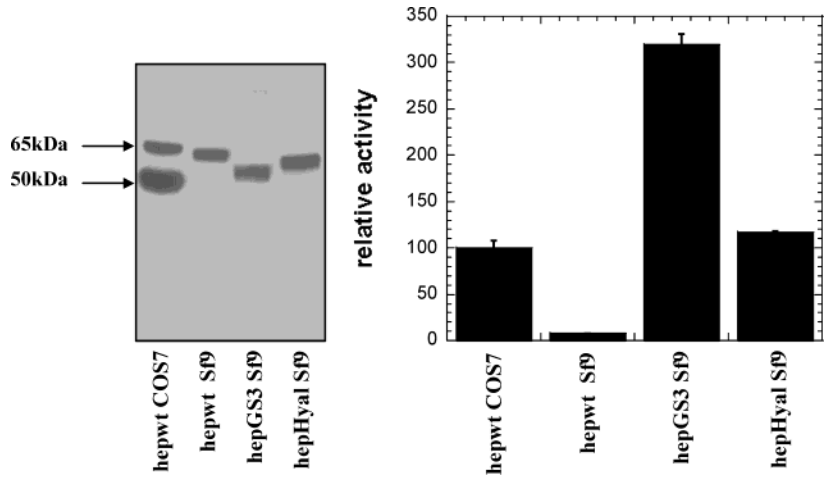

FIGURE 4: Western blot analysis of the correctly processed wild-type heparanase produced in COS7 cells or wild-type heparanase and single-chain constructs expressed in Sf9 cells (left). Heparanase activity of the same samples using the radiometric assay (right). The specific activity of wild-type heparanase and single-chain constructs expressed in Sf9 cells is normalized against that of the correctly processed wild-type heparanase produced in COS7 cells and reported as relative activity. Data and standard deviations (error bars) were calculated by linear regression analysis from triplicates of three different enzyme concentrations.

(Figure 4, left) or tested for heparanase activity (Figure 4, right).

Western blot analysis showed that wild-type heparanase, when expressed in insect cells, appears as a single band of ~65 kDa, confirming that in this expression system the heparanase precursor does not undergo proteolytic processing (Figure 4). Moreover, both radiometric (Figure 4) and fluorimetric assays (data not shown) revealed that unprocessed wild-type heparanase is virtually inactive in cleaving heparan sulfate. In contrast, both single-chain constructs hepGS3 and hepHyal, when expressed in insect cells, are enzymatically active (Figure 4). hepGS3 and hepHyal gave a single band on both Coomassie blue-stained gels or by Western blot analysis (Figure 4), suggesting that they were not processed in insect cells and that the heparan sulfate degrading activity we observed was associated with the unprocessed single-chain protein. Similar results were obtained by analyzing wild-type heparanase, hepGS3, and

hepHyal purified from the medium of the infected insect cells (not shown). When cell extracts or medium supernatants of Sf9 cells infected with hepHyal-encoding baculovirus were chromatographed on a HyperD heparin column, heparanase activity cochromatographed with the single-chain protein (not shown). As a further control, we subjected single-chain hepGS3 from Sf9 cell culture media to three subsequent chromatographic steps: (1) chromatography on a HyperD heparin column, (2) ion exchange chromatography on a source S column, and (3) size exclusion chromatography on a Superdex 75 column. Heparanase activity was copurified over all steps with the single-chain protein (not shown). We conclude that heparanase activity is indeed associated with the unprocessed single-chain proteins.

Characterization of the Enzymatic Activity of Single-Chain Proteins. We went on to characterize the activity of our active single-chain constructs in more detail. First, we analyzed the chromatographic profile of the FITC-HS hydrolysis products generated by either correctly processed wild-type protein produced in COS7 cells or single-chain constructs produced in insect cells (Figure 5A−C). The chromatographic analysis was carried out at different time points, chosen within the linear range of the reaction (up to 1 h; see the insets) and after incubation for 6 h, when the reaction was complete. Very similar profiles were obtained, suggesting that no gross alterations in substrate specificity occur in either hepGS3 or hepHyal with respect to the wild-type processed heterodimer. We noticed that in all cases extrapolation of the linear phase of the reaction time course to zero gave a measurable *y*-axis intercept (Figure 5A−C, insets). This behavior could possibly result from a processive hydrolysis reaction and deserves a more detailed investigation.

We observed that the enzymatic activity of wild-type heparanase is significantly affected by ionic strength. The ionic strength dependence of the wild type produced in COS7 cells and single-chain proteins produced in insect cells proved to be very similar (Figure 6A), again suggesting similar substrate recognition mechanisms of all tested proteins. As a further indication of the substantial conservation of active site architecture, wild-type control and single-chain proteins were inhibited with very similar potencies by heparin (Figure 6B) and heparin titration curves of hydrolytic activity were superimposable. Finally, very similar pH optima of enzymatic activity were found for all enzymes that were tested (Figure 6C). We notice, however, that the shapes of the activity titration curves as a function of pH slightly differ, possibly indicating some more subtle differences. These differences are difficult to dissect using a macromolecular substrate such as heparan sulfate and should be explored in more detail using chemically defined oligosaccharide substrates.

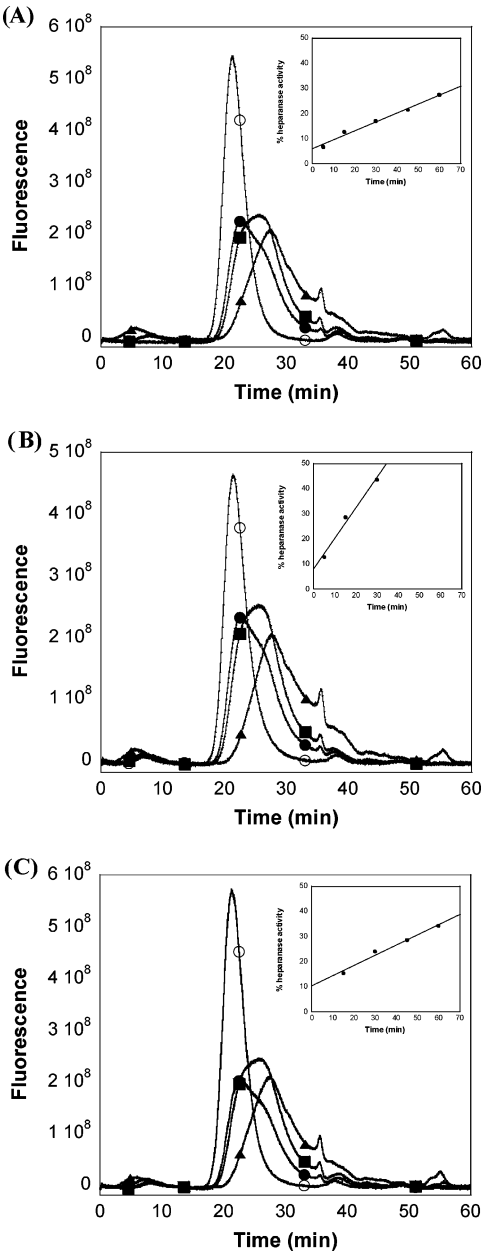

FIGURE 5: Chromatographic profiles of the FITC-HS hydrolysis products generated by correctly processed wild-type heparanase produced in COS7 cells (A) after incubation for 0 min (○), 15 min (●), 60 min (■), and 6 h (▲); hepGS3 single-chain protein produced in insect cells (B) after incubation for 0 min (○), 5 min (●), 15 min (■), and 6 h (▲); and hepHyal single-chain protein produced in insect cells (C) after incubation for 0 min (○), 15 min (●), 45 min (■), and 6 h (▲). The inset in each panel shows the time course of FITC-HS degradation by the respective heparanase construct. In the insets, heparanase activity is reported as a percentage of the maximum level of FITC-HS conversion observed after digestion for 6 h.

DISCUSSION

To investigate in more detail the role of proteolytic processing in the activation process of heparanase, we engineered TEV protease cleavage sites in the proximity of the junctions between positions 109 and 110 and 157 and 158 of the 65 kDa heparanase precursor. Using purified proteins, we were able to successfully recapitulate heparanase activation in vitro, showing that (1) processing at the junction of residues 109 and 110 alone is insufficient, (2) processing at both junctions between residues 109 and 110 and 157 and 158 does lead to activation, and (3) the activation switch is solely mediated by the presence or absence of the 6 kDa fragment and does not require additional components. This fragment appears to tolerate considerable engineering (introduction of TEV consensus sites) without losing its ability to repress heparanase activity, but it was shown not to inhibit active heparanase when added as a synthetic peptide in trans (*35*).

Multiple-sequence alignments and secondary structure prediction lead to a model of the human heparanase accord-

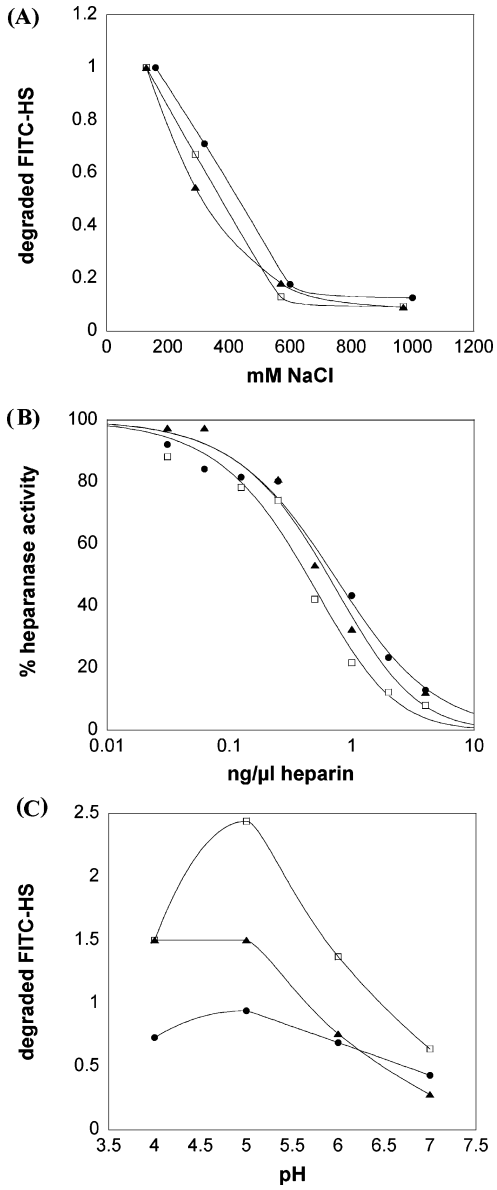

FIGURE 6: Ionic strength dependence (A), inhibition by heparin (B), and pH dependence (C) of wild-type heparanase produced in COS7 cells (●), hepGS3 (□), and hepHyal (▲) single-chain constructs produced in insect cells using the fluorimetric activity assay. The amount of degraded FITC-HS was calculated from HPLC chromatograms by measuring the increase in the amount of lower-molecular mass heparan sulfate species compared with the intact FITC-HS and quantified by peak area integration. In the heparin titration experiment, the following IC_{50} values were obtained: 0.9 ng/μL for hepwt, 1.1 ng/μL for hepGS3, and 1.5 ng/μL for hepHyal.

ing to which the protein adopts a TIM barrel fold, as found in several glycosidases (*37*). This common fold motif usually consists of eight alternating α-helices and β-strands. Within the heparanase 50 kDa fragment, clear homology is observed for only six α/β units, suggesting either a departure from the classical $(\alpha/\beta)_8$-TIM barrel fold or that other parts of the protein contribute the missing units. Our aim was to gain a better understanding of the molecular architecture of heparanase and in particular of the requirement for the 8 kDa subunit in the catalytic activity. We showed that structure predictions indicate the presence of a $\beta/\alpha/\beta$ element in the 8 kDa fragment in addition to a conserved arginine residue on the second β-strand, which interacts with a catalytic Glu in other TIM barrel glycosyl hydrolases, suggesting that this fragment is indeed contributing the missing units of the TIM barrel fold. According to this model, the excised 6 kDa fragment would link the β-strand and the α-helix within the second β/α structural unit. Taking into account that the excised 6 kDa fragment has inhibitory properties not shared by topologically equivalent linkers present in other TIM barrel hydrolases, we set out to substitute the 6 kDa fragment with other linker sequences in an attempt to generate constitutively active, single-chain heparanase molecules that would validate our model. On the basis of multiple-sequence alignments, we came up with several possible linkers. Our results show that the grafting of a loop found in a topologically homologous position in *H. manillensis* hyaluronidase on human heparanase indeed resulted in a constitutively active single-chain enzyme, in line with the concept of the 8 kDa fragment contributing the missing structural units of the TIM barrel fold. The hyaluronidase loop connection quite selectively conferred activity to the single-chain construct: with one exception (the hepGS3 construct), all other fusions or insertions lead to either inactive or unstable proteins. Specifically, the replacement of the hyaluronidase loop sequence with a $(Gly\text{-}Ser/Ala)_4$ repeat failed to yield an active heparanase, despite the very similar length of the connecting sequence.

Our data are consistent with heparanase adopting a $(\alpha/\beta)_8$-TIM barrel fold with the insertion domain located inside the second β/α unit of the barrel. As in many other glycosylases in which β/α units 1 and 2 seem to participate in substrate binding, one can speculate that the presence of the complete insertion domain on unit 2 is likely to prevent substrate binding. Heparanase is known to require at least tetrasaccharide substrates (*45*), thus implying a rather extended binding site. From the structures of several TIM barrel glycosylases in complex with substrate analogues, the loop regions following strand 1 and strand 2 have been implicated in substrate recognition, and consequently, it is reasonable to assume that in heparanase the extra portion present in the loop following strand 2 impedes substrate binding, and consequently enzymatic activity. Still, these considerations are rather speculative, and the exact mechanism by which the 6 kDa insertion loop and its proteolytic removal affect the enzymatic activity of heparanase will have to be addressed in a more direct way by elucidating the three-dimensional structures of the precursor and heterodimeric forms of the enzyme.

Heparanase, like all extracellular matrix remodeling enzymes, must be tightly regulated to ensure that it exerts its function only where and when required. The fact that heparanase is initially synthesized in a latent form with very low enzymatic activity and is activated after proteolytic processing could provide a mechanism that could ensure that the activation of this protein occurs only in particular compartments. Besides this, further mechanisms could intervene to finely modulate the behavior of this protein, for example, the pH of the microenvironment. Several studies reported that heparanase exhibits maximal endoglycosidase activity between pH 5.0 and 6.0 and shows very little enzymatic activity at the physiological pH 7 (*32*, *46*, *47*). It has also been suggested that this pH dependence profile could reflect a mechanism by which the status of the extracellular environment regulates the behavior of this protein (*32*, *33*,

48). Once localized on the cell surface, at the physiological pH, heparanase could function as a cell adhesion molecule, and under more acidic conditions, which exist in the proximity of tumors and inflammation sites, it could exert its endoglycosidase activity on HS (*32*, *33*).

Excision of the intervening 6 kDa fragment and generation of an active heterodimer might provide another level of control, potentially through inactivation by heterodimer dissociation. We found that, upon proteolytic processing by TEV protease, purified, recombinant heparanase harboring two TEV cleavage sites was rather unstable under diluted conditions, but was significantly stabilized upon addition of heparan sulfate (not shown). It is at least conceivable that similar mechanisms, building on the modulation of heterodimer stability, may contribute to confining the activity of heparanase in space and time. It would be interesting to investigate how the heterodimer stability of the wild-type enzyme is affected by different physicochemical conditions of the extracellular milieu.

The data reported herein have some practical implications in the assessment of heparanase as a novel anticancer or anti-inflammatory target. In fact, the possibility of producing large amounts of active, recombinant protein will facilitate the setup of screening assays and the determination of the three-dimensional structure of heparanase. We have shown that the properties of our single-chain constructs are identical to those of the wild-type heterodimeric protein with regard to (1) the pattern of cleavage fragments generated from high-molecular mass labeled HS, (2) the inhibition of this process by heparin, (3) the ionic strength dependence of enzymatic activity, and (4) its pH optimum. From these findings, we conclude that our single-chain heparanases may well be suited for the identification of novel heparanase inhibitors in high throughput screening campaigns.

ACKNOWLEDGMENT

We express our gratitude to Gessica Filocamo for skillful advice and many helpful discussions.

REFERENCES

1. Vlodavsky, I., Friedmann, Y., Elkin, M., Aingorn, H., Atzmon, R., Ishai-Michaeli, R., Bitan, M., Pappo, O., Peretz, T., Micha, I., Spector, L., and Pecker, I. (1999) Mammalian heparanase: gene cloning, expression and function in tumor progression and metastasis, *Nat. Med. 5*, 793−802.
2. Hulett, M. D., Freeman, C., Hamdorf, B. J., Baker, R. T., Harris, M. J., and Parish, C. R. (1999) Cloning of mammalian heparanase, an important enzyme in tumor invasion and metastasis, *Nat. Med. 5*, 803−809.
3. Kussie, P. H., Hulmes, J. D., Ludwig, D. L., Patel, S., Navarro, E. C., Seddon, A. P., Giorgio, N. A., and Bohlen, P. (1999) Cloning and functional expression of a human heparanase gene, *Biochem. Biophys. Res. Commun. 261*, 183−187.
4. Toyoshima, M. T., and Nakajima, M. (1999) Human heparanase. Purification, characterization, cloning, and expression, *J. Biol. Chem. 274*, 24153−24160.
5. Kjellen, L., and Lindahl, U. (1991) Proteoglycans: structures and interactions, *Annu. Rev. Biochem. 60*, 443−475.
6. David, G. (1993) Integral membrane heparan sulfate proteoglycans, *FASEB J. 7*, 1023−1030.
7. Iozzo, R. V. (1998) Matrix proteoglycans: from molecular design to cellular function, *Annu. Rev. Biochem. 67*, 609−652.
8. Bernfield, M., Gotte, M., Park, P. W., Reizes, O., Fitzgerald, M. L., Lincecum, J., and Zako, M. (1999) Functions of cell surface heparan sulfate proteoglycans, *Annu. Rev. Biochem. 68*, 729−777.
9. Esko, J. D., and Lindahl, U. (2001) Molecular diversity of heparan sulfate, *J. Clin. Invest. 108*, 169−173.
10. Turnbull, J., Powell, A., and Guimond, S. (2001) Heparan sulfate: decoding a dynamic multifunctional cell regulator, *Trends Cell Biol. 11*, 75−82.
11. Vlodavsky, I., Bar-Shavit, R., Korner, G., and Fuks, Z. (1993) in *Basement Membranes: Cellular and Molecular Aspects* (Rohrbach, D. H., and Timpl, R., Eds.) pp 327−343, Academic Press, Orlando, FL.
12. Vlodavsky, I., Miao, H. Q., Medalion, B., Danagher, P., and Ron, D. (1996) Involvement of heparan sulfate and related molecules in sequestration and growth promoting activity of fibroblast growth factor, *Cancer Metastasis Rev. 15*, 177−186.
13. Sasisekharan, R., and Venkataraman, G. (2000) Heparin and heparan sulfate: biosynthesis, structure and function, *Curr. Opin. Chem. Biol. 4*, 626−631.
14. Pillarisetti, S., Paka, I., Sasaki, A., Vanni-Reyes, T., Yin, B., Parthasarathy, N., Wagner, W. D., and Goldberg, I. J. (1997) Endothelial cell heparanase modulation of lipoprotein lipase activity. Evidence that heparan sulfate oligosaccharide is an extracellular chaperone, *J. Biol. Chem. 272*, 15753−15759.
15. Lyon, M., and Gallagher, J. T. (1998) Bio-specific sequences and domains in heparan sulphate and the regulation of cell growth and adhesion, *Matrix Biol. 17*, 485−493.
16. Woods, A., Oh, E. S., and Couchman, J. R. (1998) Syndecan proteoglycans and cell adhesion, *Matrix Biol. 17*, 477−483.
17. Sperinde, G. V., and Nugent, M. A. (1998) Heparan sulfate proteoglycans control intracellular processing of bFGF in vascular smooth muscle cells, *Biochemistry 37*, 13153−13164.
18. Chang, Z., Meyer, K., Rapraeger, A. C., and Friedl, A. (2000) Differential ability of heparan sulfate proteoglycans to assemble the fibroblast growth factor receptor complex in situ, *FASEB J. 14*, 137−144.
19. Perrimon, N., and Bernfield, M. (2000) Specificities of heparan sulphate proteoglycans in developmental processes, *Nature 404*, 725−728.
20. Sasisekharan, R., Shriver, Z., Venkataraman, G., and Narayanasami, U. (2002) Roles of heparan-sulphate glycosaminoglycans in cancer, *Nat. Rev. Cancer 2*, 521−528.
21. Liu, D., Shriver, Z., Qi, Y., Venkataraman, G., and Sasisekharan, R. (2002) Dynamic regulation of tumor growth and metastasis by heparan sulfate glycosaminoglycans, *Semin. Thromb. Hemostasis 28*, 67−78.
22. Nakajima, M., Irimura, T., and Nicolson, G. L. (1988) Heparanases and tumor metastasis, *J. Cell. Biochem. 36*, 157.
23. Vlodavsky, I., Eldor, A., Haimovitz-Friedman, A., Matzner, Y., Ishai-Michaeli, R., Lider, O., Naparstek, Y., Cohen, I. R., and Fuks, Z. (1992) Expression of heparanase by platelets and circulating cells of the immune system: possible involvement in diapedesis and extravasation, *Invasion Metastasis 12*, 112−127.
24. Dempsey, L. A., Brunn, G. J., and Platt, J. L. (2000) Heparanase, a potential regulator of cell−matrix interactions, *Trends Biochem. Sci. 25*, 349−351.
25. Parish, C. R., Freeman, C., and Hulett, M. D. (2001) Heparanase: a key enzyme involved in cell invasion, *Biochim. Biophys. Acta 1471*, M99−M108.
26. Vlodavsky, I., and Friedmann, Y. (2001) Molecular properties and involvement of heparanase in cancer metastasis and angiogenesis, *J. Clin. Invest. 108*, 341−347.
27. Vlodavsky, I., Mohsen, M., Lider, O., Svahn, C. M., Ekre, H. P., Vigoda, M., Ishai-Michaeli, R., and Peretz, T. (1994) Inhibition of tumor metastasis by heparanase inhibiting species of heparin, *Invasion Metastasis 14*, 290−302.
28. Uno, F., Fujiwara, T., Takata, Y., Ohtani, S., Katsuda, K., Takaoka, M., Ohkawa, T., Naomoto, Y., Nakajima, M., and Tanaka, N. (2001) Antisense-mediated suppression of human heparanase gene expression inhibits pleural dissemination of human cancer cells, *Cancer Res. 61*, 7855−7860.
29. Elkin, M., Ilan, N., Ishai-Michaeli, R., Friedmann, Y., Papo, O., Pecker, I., and Vlodavsky, I. (2001) Heparanase as mediator of angiogenesis: mode of action, *FASEB J. 15*, 1661−1663.
30. Folkman, J., Klagsbrun, M., Sasse, J., Wadzinski, M., Ingber, D., and Vlodavsky, I. (1988) A heparin-binding angiogenic protein—basic fibroblast growth factor—is stored within basement membrane, *Am. J. Pathol. 130*, 393−400.
31. Goldshmidt, O., Zcharia, E., Abramovitch, R., Metzger, S., Aingorn, H., Friedmann, Y., Schirrmacher, V., Mitrani, E., and Vlodavsky, I. (2002) Cell surface expression and secretion of

heparanase markedly promote tumor angiogenesis and metastasis, *Proc. Natl. Acad. Sci. U.S.A. 99*, 10031−10036.

32. Gilat, D., Hershkoviz, R., Goldkorn, I., Cahalon, L., Korner, G., Vlodavsky, I., and Lider, O. (1995) Molecular behavior adapts to context: heparanase functions as an extracellular matrix-degrading enzyme or as a T cell adhesion molecule, depending on the local pH, *J. Exp. Med. 181*, 1929−1934.
33. Goldshmidt, O., Zcharia, E., Cohen, M., Aingorn, H., Cohen, I., Nadav, L., Katz, B. Z., Geiger, B., and Vlodavsky, I. (2003) Heparanase mediates cell adhesion independent of its enzymatic activity, *FASEB J. 17*, 1015−1025.
34. Fairbanks, M. B., Mildner, A. M., Leone, J. W., Cavey, G. S., Mathews, W. R., Drong, R. F., Slightom, J. L., Bienkowski, M. J., Smith, C. W., Bannow, C. A., and Heinrikson, R. L. (1999) Processing of the human heparanase precursor and evidence that the active enzyme is a heterodimer, *J. Biol. Chem. 274*, 29587−29590.
35. McKenzie, E., Young, K., Hircock, M., Bennett, J., Bhaman, M., Felix, R., Turner, P., Stamps, A., McMillan, D., Saville, G., Ng, S., Mason, S., Snell, D., Schofield, D., Gong, H., Townsend, R., Gallagher, J., Page, M., Parekh, R., and Stubberfield, C. (2003) Biochemical characterization of the active heterodimer form of human heparanase (Hpa1) protein expressed in insect cells, *Biochem. J. 373*, 423−435.
36. Levy-Adam, F., Miao, H. Q., Heinrikson, R. L., Vlodavsky, I., and Ilan, N. (2003) Heterodimer formation is essential for heparanase enzymatic activity, *Biochem. Biophys. Res. Commun. 308*, 885−891.
37. Hulett, M. D., Hornby, J. R., Ohms, S. J., Zuegg, J., Freeman, C., Gready, J. E., and Parish, C. R. (2000) Identification of active-site residues of the pro-metastatic endoglycosidase heparanase, *Biochemistry 39*, 15659−15667.
38. Altschul, S. F., Madden, T. L., Schaffer, A. A., Zhang, J., Zhang, Z., Miller, W., and Lipman, D. J. (1997) Gapped BLAST and PSI-BLAST: a new generation of protein database search programs, *Nucleic Acids Res. 25*, 3389−3402.
39. Jones, D. T. (1999) Protein secondary structure prediction based on position-specific scoring matrices, *J. Mol. Biol. 292*, 195−202.
40. Chenna, R., Sugawara, H., Koike, T., Lopez, R., Gibson, T. J., Higgins, D. G., and Thompson, J. D. (2003) Multiple sequence alignment with the Clustal series of programs, *Nucleic Acids Res. 31*, 3497−3500.
41. Galtier, N., Gouy, M., and Gautier, C. (1996) SEAVIEW and PHYLO_WIN: two graphic tools for sequence alignment and molecular phylogeny, *Comput. Appl. Biosci. 12*, 543−548.
42. Freeman, C., and Parish, C. R. (1997) A rapid quantitative assay for the detection of mammalian heparanase activity, *Biochem. J. 325*, 229−237.
43. Nakajima, M., Irimura, T., and Nicolson, G. L. (1986) A solid-phase substrate of heparanase: its application to assay of human melanoma for heparan sulfate degradative activity, *Anal. Biochem. 157*, 162−171.
44. Kordowicz, M., Guessow, D., Hofmann, U., Pacuszka, T., and Gardas, A. (2002) World Patent WO0077221.
45. Okada, Y., Yamada, S., Toyoshima, M., Dong, J., Nakajima, M., and Sugahara, K. (2002) Structural recognition by recombinant human heparanase that plays critical roles in tumor metastasis. Hierarchical sulfate groups with different effects and the essential target disulfated trisaccharide sequence, *J. Biol. Chem. 277*, 42488−42495.
46. Graham, L. D., and Underwood, P. A. (1996) Comparison of the heparanase enzymes from mouse melanoma cells, mouse macrophages, and human platelets, *Biochem. Mol. Biol. Int. 39*, 563−571.
47. Freeman, C., and Parish, C. R. (1998) Human platelet heparanase: purification, characterization and catalytic activity, *Biochem. J. 330*, 1341−1350.
48. Ihrcke, N. S., Parker, W., Reissner, K. J., and Platt, J. L. (1998) Regulation of platelet heparanase during inflammation: role of pH and proteinases, *J. Cell. Physiol. 175*, 255−267.

BI030203A